LAJSBA
LATIN AMERICAN JOURNAL OF SEDIMENTOLOGY AND BASIN ANALYSIS | VOLUME 28 (2) 2021, 99-118

FOSSIL BUBBLE STRUCTURE RELATED TO MICROBIAL ACTIVITY COEVAL WITH THE MIDDLE EDIACARAN OCEANIC OXYGENATION EVENT IN THE TANDILIA SYSTEM

María Julia Arrouy [1], Lucía E. Gómez-Peral [2-3], Victoria Penzo [2], Camila Ferreyra [2-4], Daniel G. Poiré [2-3]*

[1] Instituto de Hidrología de Llanuras "Dr. E. J. Usunoff"- CONICET- Argentina. jarrouy@illha.org.ar
[2] Centro de Investigaciones Geológicas (CIG-CONICET-UNLP) Diagonal 113, Nº 275, La Plata, Argentina.
[3] Cátedras de Sedimentología y de Rocas Sedimentarias, Facultad de Ciencias Naturales y Museo, Universidad Nacional de La Plata, Calle 122 y 60, 1900, La Plata, Buenos Aires, Argentina.
[4] Cátedra de Paleontología I, Facultad de Ciencias Naturales y Museo, Universidad Nacional de La Plata, Calle 122 y 60, 1900, La Plata, Buenos Aires, Argentina.

ARTICLE INFO

Article history
Received May 18, 2020
Accepted September 21, 2021
Available online October 1, 2021

Handling Editor
Fernando Gómez

Keywords
Loma Negra Formation
Limestones
MISS
Photosynthesis
Oxygen release

ABSTRACT

The well-preserved limestone succession, Loma Negra Formation (~40 m), in the Tandilia System was deposited in a shallow carbonate ramp under low energy conditions. The evolution in the depositional settings of the unit was indicated as deepening upwards varying from shallow-middle to outer ramp environment. The limestone fabric is assumed as the product of biologically controlled precipitation of micrite, where the terrigenous supply was limited. From detailed meso- and microscopic descriptions it is possible to recognize microbially induced sedimentary structures 'MISS' represented by typical microtextures related to microbial activity that appear represented throughout the entire formation. In addition, micro-stromatolites are observed in the unit associated with the microbial mats showing micro-columnar conical to domical morphologies.

In the basal and middle Loma Negra Formation, hemispherical structures are recognized in the bed-tops and interpreted as bubbles-like and gas escape features associated with the microbial mat interaction. Their morphology is compared with oxygen bubbles produced by modern experimental modelling with photosynthetic cyanobacteria microbial mats. Moreover, hemispherical structures are associated with increasing gas pressure lifting grains and the organic components to the surface.

This paper provides evidence to understand the possible causal relationship between microbial activity and seawater oxygenation. The high oxygen production revealed by geochemistry proxies and here proposed as probably associated with photosynthetic microbial activity might be a plausible explanation for the record of the documented Middle Ediacaran Oceanic Oxygenation Event in the Loma Negra Formation.

INTRODUCTION

The extensive marine connection of the interior seas in the southwestern Gondwana context and the marginal and oceanic basins, known as the Clymene Ocean (Warren *et al.*, 2014), provided the ideal

conditions for deposition of shallow carbonate facies and microbialites during the Ediacaran Period. This linked palaeogeographic scenario also explains the widely recorded positive $\delta^{13}C$ values related to ~580 Ma carbonate successions (Halverson *et al.*, 2005; Macdonald *et al.*, 2009; Cui *et al.*, 2015; Gómez-Peral *et al.*, 2018). The positive $\delta^{13}C$ values suggest high rates of organic productivity in those basins, argued as a consequence of microscopic algae and cyanobacteria photosynthesis (Lyons *et al.*, 2014).

The microbial communities have dominated Earth's surface for most of its history; they emerged in the Proterozoic oceans and inhabited various geological environments and played a decisive role in releasing oxygen (Noffke *et al.*, 2001, 2003, 2013). Several investigations have been conducted on oxygenic photosynthesis in modern microbial mats (e.g. Bosak *et al.*, 2009, 2010; Mata *et al.*, 2012; Homann *et al.*, 2015; Sallstedt *et al.*, 2018), but evidence for oxygenic photosynthesis in Precambrian rocks as probable causal of oxygenation events is still under rigorous debate.

The geological record of microscopic life consists mainly of microbially influenced-induced sedimentary features. In the Precambrian era, such mats colonized environments where their life cycle requirements were suitable and more frequently recognized in siliciclastic rocks (e.g., Schieber, 1998, 1999; Gehling, 1999; Gerdes *et al.*, 2000; Eriksson *et al.*, 2000, 2010; Noffke *et al.*, 2001, 2003, 2013; Schieber *et al.*, 2007; Banerjee *et al.*, 2014; Sarkar *et al.*, 2014a, 2016;). Nevertheless, reports of such features from carbonate deposits are rare and limited (Shi *et al.*, 2008; Luo *et al.*, 2013; Zhao *et al.*, 2020).

Microbial mats are organic-rich layers developed by microbes and their extracellular polymeric substances through trapping and binding sediments at the water/sediment interface (Gerdes *et al.*, 2000; Noffke *et al.*, 2001, 2003). In carbonate ('biochemical') depositional environments, microbial mats induce the formation of stromatolites. In siliciclastic ('physical') environments, where mineral precipitation or cementation play no role, microbial mats form microbially induced sedimentary structures 'MISS' (MISS, *sensu* Noffke *et al.*, 1996, 2001).

On the other hand, marine biogeochemical limestones widely reflect the seawater geochemistry that appear to be independent of their age (e.g., Lyons *et al.*, 2014; Sahoo *et al.*, 2012, 2016; van Smeerdijk Hood and Wallace, 2015). The redox-sensitive trace elements in carbonates are widely considered to provide evidence for multiple oceanic oxygenation events (OOEs) in a predominantly anoxic global Ediacaran ocean (van Smeerdijk Hood and Wallace, 2015; Gómez-Peral *et al.*, 2014, 2017, 2019; Och and Shields-Zhou, 2012; Lyons *et al.*, 2014; Sahoo *et al.*, 2012, 2016; Arrouy and Gómez-Peral, 2021). During this period, three marked oceanic oxygenation events (OOEs) have been suggested: the lower (ca. 635 Ma), the middle (ca. 580 Ma), and the late (ca. 560 Ma OOE), (Sahoo *et al.*, 2012, 2016).

In this study, we focus the attention on the organic sedimentary microstructures recorded in the limestones of the Loma Negra Formation, exploring geochemical evidence for its existence and examining the case for a causal relationship between the microbial activity and the seawater oxygenation in the Ediacaran context of the Tandilia Basin.

GEOLOGICAL SETTING

The southernmost outcrops of the Río de La Plata Craton sedimentary cover are represented in Argentina by the Tandilia System, a 350 km long, northwest to southeast oriented orographic belt located in the Buenos Aires province (Fig. 1A).

The geological background of the Tandilia System can be found in previous publications (Nágera, 1940; Dalla Salda and Iñiguez, 1979; Poiré and Spalletti, 2005; Arrouy *et al.*, 2015, 2016, 2019; Hernandez *et al.*, 2017; Arrouy and Gómez-Peral, 2021; Gómez-Peral *et al.*, 2021). The basement rocks (Buenos Aires Complex, Marchese and Di Paola, 1975; Cingolani, 2011) yielded U–Pb SHRIMP crystallization ages between 2234 and 2065 Ma (Transamazonian Cycle: Hartmann *et al.*, 2002). Sm-Nd model ages vary between 2440 and 2668 Ma (Hartmann *et al.*, 2002), with an average of 2620 ± 80 Ma (Pankhurst *et al.*, 2003).

In the Olavarría area (Fig. 1B), the Neoproterozoic sedimentary cover is ~435 m thick (Poiré and Spalletti, 2005; Gómez-Peral et. al., 2007, 2011; Arrouy *et al.*, 2015) and is represented by the Sierras Bayas and La Providencia groups (Fig. 1C). The Sierras Bayas Group is separated from the overlain La Providencia Group by an erosional unconformity related to eustatic sea-level fall (Poiré *et al.*, 2018).

The Sierras Bayas Group is subdivided in Villa Mónica, Colombo, Cerro Largo, Olavarría and Loma Negra Formations (Iñiguez, 1999; Poiré and Spalletti,

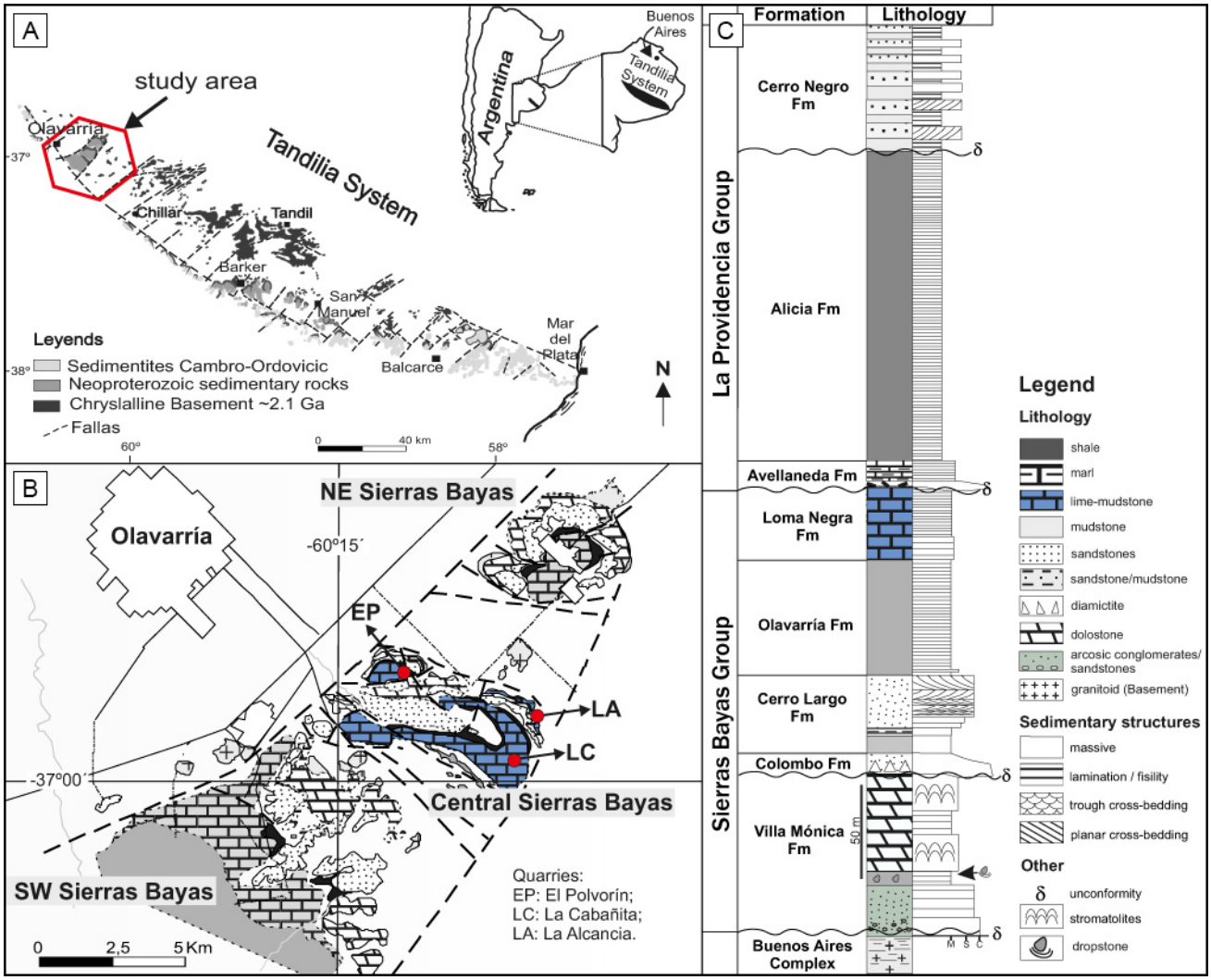

Figure 1. a) Study area in the Tandilia System (Buenos Aires Province, Argentina). **b)** Geological map of the Sierras Bayas, Olavarría region (north-western part of the Tandilia System. Modified after Iñíguez, 1999; Gómez-Peral *et al*., 2014). Quarries sections: EP: El Polvorín, LC: La Cabañita, LA: La Alcancía. **c)** Schematic representation of the Sierras Bayas and La Providencia Groups (after Gómez-Peral *et al*., 2014; Arrouy and Gómez-Peral, 2021).

2005; Gómez-Peral, 2008). In this study, we focus on the youngest depositional sequence of the Sierras Bayas Group, the Loma Negra formation.

In the Olavarría area, the Loma Negra Formation is well exposed in quarry walls. It comprises a very homogeneous carbonate deposit, ~40 m thick, almost exclusively mud limestone (Fig. 2). The unit is divided into two sections: the basal is characterized by reddish- or greenish- carbonate mudstones up to 8 m thick, constituted by micritic calcite with ~20% of terrigenous components (mainly quartz and scarce clay minerals), and show planar lamination interbedded with wavy, rippled and cross-laminated limestones (Fig. 2A, B, C). The middle and upper sections (up to 33 m thick, Fig.2D-E), are composed of black thin laminated mudstones with ~ 90% $CaCO_3$, with very scarce terrigenous (Gómez-Peral *et al*., 2019). The Loma Negra Formation was interpreted as developed in a carbonate platform type ramp environment. This cycle of sedimentation begins with the installation of a carbonate ramp with wave influence, under favourable conditions for deposition of very fine carbonate with scarce to moderate terrigenous supply. After that, the middle and upper sections of the Loma Negra Formation had been deposited in an outer ramp environment under low energy conditions (Gómez-Peral *et al*., 2018).

The age of the Loma Negra Formation was debated but latest suggested as 580–590 Ma, by the $\delta^{13}C$ (+2.2 to +4.5‰) and $^{87}Sr/^{86}Sr$ (0.7069 up to 0.7080)

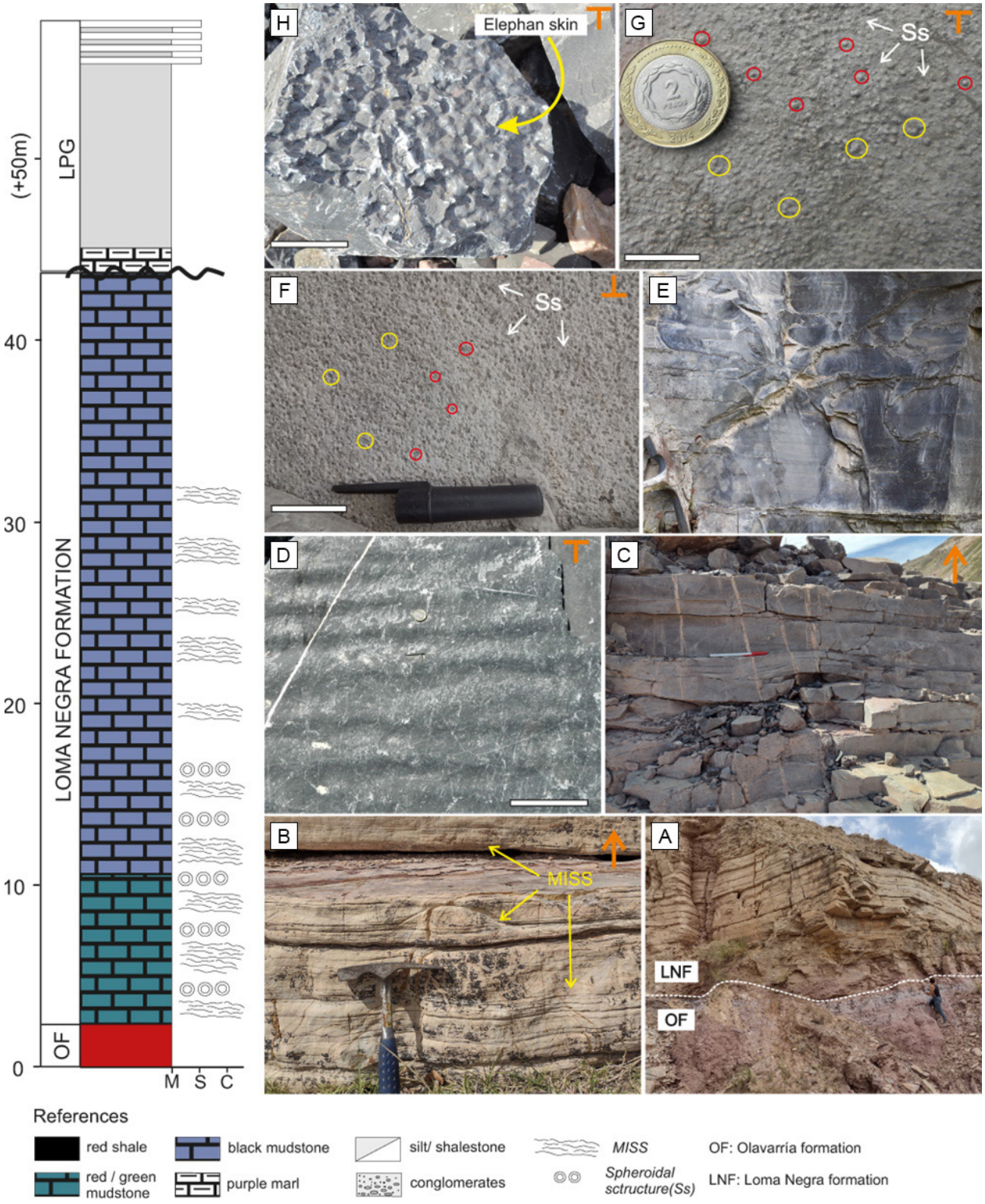

Figure 2. Field photographs from the Loma Negra Formation. **a)** The contact between Olavarría Formation and Loma Negra Formation marked with a dotted white line. **b)** Microbial mat laminated (MISS) in the reddish or greenish lime mudstone facies (MC). **c)** Laminated mudstones (MC) with ripple. **d)** Ripple marks on a bedding plane. **e)** The black laminated limestone facies (MB). **f)** Hemispherical microstructures in negative epirelief, (individual = red circle; coalescent = yellow circle). **g)** Hemispherical microstructures in positive epirelief. **h)** Elephant Skin Structure developed on an upper bedding surface limestone. The scale bar in D is 5 cm, 2 cm in F, 1 cm in G and 5 cm in H. The hammer in B is 33 cm long. ⊤ for top bedding surface view, ⊥ for bottom bedding surface view, and ↑ for stratigraphic top.

(Gómez-Peral *et al.*, 2018). In the overlying unit, Avellaneda Formation, a marked negative excursion in $\delta^{13}C$ was denoted, varying from +2.8 to −3.6‰, which was considered the cooling response during a glaciation ~580 Ma (Gómez-Peral *et al.*, 2018). In addition, Arrouy *et al.* (2016) reported Aspidella fossils from the overlying Cerro Negro Formation, suggesting a late Ediacaran age for this unit.

The biomarker distribution in the micritic limestones of the Loma Negra Formation in the Barker area had been studied by Bagnaud-Velazquez *et al.* (2013). These authors recognized, based on the occurrence of specific biomarkers, the presence of a diverse microbial community including primary producers such as cyanobacteria, phototrophic bacteria, green bacteria and some methanogenic bacteria.

In addition, postglacial phosphorite concretionary levels were reported in the basal Avellaneda Formation, just overlying the Loma Negra Formation. Such levels formed under well-oxygenated sea-floor conditions in the context of a fully ventilated ocean (Gómez-Peral *et al.*, 2019).

SAMPLING AND METHODS

Three locations in the Olavarría area were sampled, two in La Cabañita Quarry and one in La Alcancía Quarry. All the collected samples are limestones from the Loma Negra Formation. Although the entire formation was sampled, we emphasize the lower and middle sections where the organic sedimentary structures were concentrated and better recognized. The samples were stratigraphically oriented according to the protocol of Chen *et al.*, 2013 (┬ for top bedding surface view, ┴ for bottom bedding surface view, and ↑ for the stratigraphic top).

Centimetre-sized slabs samples studied were extracted from outcrops and quarry walls. In the laboratory, some samples were cut into two pieces: 1) perpendicularly to the carborundum powder-based manual grinder and 2) thin sections to be observed under a petrographic microscope. The samples rich in organic structures were scanned, photographed, and observed under the loupe. The thin sections were examined to make a detailed description of their microscopic components, textures and structures.

Samples analyzed were divided into coloured lime-mudstones (grey, reddish or greenish = MC) and black lime-mudstones (MB) that were previously characterized as two different sedimentary facies associations (cf. Gómez-Peral *et al.*, 2007; 2018; 2019).

A total of fifty (50) polished uncovered thin sections were observed and analyzed with the petrographic microscope Nikon Eclipse at the Centro de Investigaciones Geológicas, La Plata, Argentina (CIG). Thin sections (30 μm thick) were essential for characterization of sedimentary structures, texture and mineral composition.

Unprocessed chips of selected mudstones were analyzed by scanning electron microscope (SEM) to study the mineralogical and the organic structure record. Samples were air-dried to constant weight before testing and coated with gold. Each sample was studied at different magnifications (i.e. 6000, 12000 X) for optimal determination of the microstructure details. Samples were analyzed with the SEM X-ray energy-dispersive spectrometer JEOL JXA 8230 equipped with 5WDS spectrometers and a solid-state EDS detector, at the Department of Petrology at São Paulo State University (UNESP), Brazil.

Thirty-two (32) samples of lime-mudstones, seven (7) of MC and twenty-five (25) of MB were analyzed using a Perkin-Elmer Inductively Coupled Plasma mass spectrometry (ICP-MS) fitted with a Meinhardt concentric nebulizer of the Centro de Investigaciones Geológicas laboratories (CONICET-UNLP, Argentina). Minor and trace elements were concentrated from digested samples for two hours in trace metal grade 2% HNO_3 v/v added dropwise, using sufficient acid to dissolve 100% carbonate. Solutions were centrifuged and decanted to remove insoluble residue and analyzed with the ICP-MS to determine trace elements (REE presented in Table 1 were taken from Gómez-Peral *et al.*, 2019; S and P added in Table 1, and V, Cr, Co, Ni, Cu, Ba, Pb, Th, U results obtained here Table 2). Precision and reproducibility for all elements analyzed are better than 10%, based on replicate measurements of laboratory calcite and dolomite Perkin Elmer standards.

X-ray fluorescence spectrometry (XRF) measurements of major elements performed by ALS Laboratory Group (Geochemistry Canada) were included in the analysis (Table 1, modified from Gómez-Peral *et al.*, 2019).

REE plus Y (REY) concentrations were normalized relative to the standard post-Archean Australian Shale (PAAS, McLennan, 1989). Following Lawrence *et al.* (2006), the anomalies were calculated from a

Sample	La	Ce	Pr	Nd	Sm	Eu	Gd	Tb	Dy	Y	Ho	Er	Tm	Yb	Lu	La/Sm	Ce/Ce*	Eu/Eu	Pr/Pr*	ΣREE+Y	ΣREE	Gd/Gd*	Y/Ho	CaO	Al2O3	P (ppm)	S(ppm)
MC 1	0,14	0,12	0,16	0,21	0,26	0,34	0,33	0,24	0,24	0,26	0,19	0,21	0,18	0,19	0,16	0,55	0,98	3,74	0,97	36,68	29,64	0,43	36,59	46,2	2,09	1916	ni
MC 3	0,10	0,08	0,11	0,14	0,16	0,19	0,22	0,17	0,17	0,18	0,14	0,15	0,13	0,13	0,11	0,61	0,97	4,63	0,97	25,06	20,08	0,22	36,49	45,3	1,87	440	274
MC 4	0,15	0,09	0,14	0,19	0,23	0,26	0,31	0,24	0,25	0,28	0,20	0,22	0,19	0,21	0,18	0,64	0,86	3,34	1,01	33,06	25,47	0,37	38,23	45,4	1,88	86	274
MC 6	0,15	0,11	0,22	0,33	0,45	0,50	0,62	0,46	0,48	0,55	0,38	0,41	0,35	0,40	0,35	0,33	0,76	1,67	1,00	53,77	38,97	1,15	39,59	43,5	2,56	64	ni
MC 7	0,12	0,14	0,22	0,30	0,38	0,43	0,54	0,42	0,44	0,56	0,36	0,41	0,37	0,42	0,39	0,32	0,89	1,87	0,98	55,13	39,91	0,91	43,20	43,7	2,24	90	91
MC 8	0,12	0,09	0,17	0,24	0,33	0,41	0,41	0,31	0,33	0,37	0,26	0,30	0,26	0,31	0,27	0,36	0,75	2,73	1,02	38,85	28,89	0,62	38,46	46,2	2,09	134	ni
MB 12	0,10	0,08	0,13	0,18	0,23	0,33	0,30	0,24	0,24	0,29	0,20	0,22	0,19	0,20	0,18	0,44	0,84	4,05	1,02	32,10	24,27	0,37	39,99	53,2	0,76	70	183
MB 15	0,12	0,07	0,13	0,18	0,22	0,26	0,31	0,24	0,26	0,35	0,22	0,25	0,22	0,25	0,23	0,55	0,73	3,39	1,05	32,87	23,50	0,37	43,25	53,7	0,7	101	137
MB 17	0,15	0,06	0,11	0,15	0,19	0,23	0,26	0,21	0,22	0,30	0,19	0,21	0,19	0,21	0,19	0,78	0,71	4,07	1,06	28,78	20,58	0,29	44,09	52,7	0,78	114	183
MB 22	0,12	0,07	0,13	0,18	0,22	0,27	0,33	0,24	0,26	0,37	0,20	0,23	0,19	0,20	0,18	0,56	0,71	3,49	1,05	32,94	23,00	0,38	48,92	52,4	0,76	101	183
MB 26	0,12	0,06	0,12	0,16	0,20	0,27	0,30	0,23	0,25	0,36	0,21	0,24	0,21	0,23	0,20	0,59	0,68	3,98	1,06	30,99	21,25	0,34	45,84	52,9	0,62	57	183
MC 085	0,39	0,18	0,25	0,26	0,45	0,54	0,55	0,33	0,33	0,21	0,22	0,24	0,10	0,14	0,06	0,87	0,78	2,54	1,11	54,78	49,19	0,97	26,14	49,0	1,68	101	411
MB 087	0,18	0,13	0,17	0,18	0,29	0,32	0,37	0,21	0,24	0,16	0,16	0,20	0,10	0,18	0,09	0,62	0,78	3,68	1,12	35,16	30,80	0,46	27,61	50,6	0,96	92	503
MB 088	0,18	0,14	0,20	0,23	0,40	0,37	0,55	0,34	0,35	0,19	0,23	0,26	0,13	0,19	0,10	0,46	0,84	1,90	1,06	41,98	36,88	0,90	22,28	53,5	0,79	81	229
MB 089	0,14	0,09	0,10	0,11	0,15	0,12	0,23	0,12	0,16	0,14	0,10	0,15	0,06	0,13	0,05	0,94	0,91	4,82	1,05	24,69	20,99	0,18	35,91	51,7	0,8	119	229
MB 091	0,17	0,12	0,23	0,25	0,39	0,35	0,53	0,38	0,42	0,30	0,32	0,36	0,26	0,32	0,25	0,44	0,57	1,62	1,24	44,56	36,43	0,89	25,62	51,3	0,73	101	229
MB 092	0,27	0,14	0,28	0,32	0,50	0,43	0,71	0,45	0,47	0,31	0,33	0,36	0,20	0,27	0,17	0,54	0,57	1,31	1,23	55,00	46,63	1,39	25,97	51,9	0,88	106	46
MB 093	0,12	0,09	0,18	0,20	0,32	0,27	0,43	0,28	0,31	0,22	0,23	0,26	0,15	0,22	0,15	0,39	0,57	2,11	1,23	33,90	27,87	0,60	26,84	52,2	0,75	84	46
MB 094	0,17	0,07	0,10	0,11	0,17	0,16	0,26	0,15	0,20	0,15	0,14	0,18	0,08	0,16	0,08	0,98	0,73	4,23	1,13	25,04	21,03	0,24	29,21	51,5	0,94	81	46
MB 095	0,18	0,11	0,22	0,27	0,47	0,45	0,67	0,43	0,47	0,29	0,34	0,38	0,23	0,30	0,19	0,38	0,60	1,54	1,17	45,41	37,54	1,24	23,23	52,4	0,77	77	137
MB 096	0,14	0,06	0,11	0,12	0,18	0,18	0,28	0,17	0,21	0,17	0,14	0,18	0,08	0,16	0,08	0,76	0,67	3,99	1,17	24,57	20,08	0,27	31,68	52,9	0,76	106	137
MB 097	0,11	0,06	0,11	0,11	0,18	0,16	0,28	0,16	0,20	0,16	0,14	0,18	0,08	0,15	0,07	0,61	0,57	3,94	1,24	22,32	18,10	0,26	30,93	51,9	0,77	97	137
MB 098	0,10	0,05	0,10	0,11	0,17	0,18	0,27	0,16	0,21	0,17	0,15	0,19	0,09	0,16	0,08	0,57	0,54	4,52	1,25	21,32	16,82	0,25	30,95	52,2	0,7	86	229
MB 099	0,20	0,07	0,15	0,16	0,27	0,26	0,41	0,26	0,31	0,22	0,23	0,28	0,17	0,24	0,16	0,73	0,53	2,54	1,25	33,20	27,16	0,51	27,11	51,7	0,8	84	274
MB 100	0,15	0,07	0,14	0,15	0,25	0,24	0,37	0,23	0,27	0,20	0,19	0,23	0,12	0,19	0,11	0,62	0,56	2,91	1,24	29,34	23,98	0,43	28,64	51,1	0,82	110	183
MB 101	0,15	0,08	0,17	0,19	0,33	0,31	0,46	0,31	0,37	0,27	0,28	0,34	0,22	0,30	0,22	0,46	0,55	2,08	1,23	35,63	28,46	0,67	25,82	50,7	0,85	108	137
MB 102	0,15	0,09	0,17	0,20	0,34	0,31	0,45	0,29	0,33	0,22	0,23	0,27	0,15	0,22	0,14	0,43	0,59	2,18	1,20	34,55	28,65	0,66	25,91	50,4	0,86	84	137
MB 103	0,16	0,08	0,17	0,19	0,32	0,32	0,48	0,33	0,38	0,30	0,29	0,35	0,23	0,32	0,23	0,50	0,54	2,12	1,24	37,10	28,96	0,68	28,14	50,9	0,78	84	46
MB 104	0,19	0,10	0,21	0,25	0,44	0,41	0,63	0,42	0,47	0,34	0,34	0,40	0,25	0,34	0,24	0,44	0,53	1,51	1,23	45,77	36,53	1,12	27,10	52,7	0,72	73	274
MB 105	0,11	0,09	0,17	0,20	0,32	0,31	0,49	0,32	0,37	0,29	0,28	0,34	0,22	0,30	0,21	0,35	0,56	2,11	1,23	35,56	27,83	0,68	27,43	50,9	0,93	75	137
MB 106	0,22	0,09	0,22	0,27	0,50	0,45	0,71	0,49	0,53	0,33	0,39	0,44	0,29	0,37	0,29	0,45	0,49	1,30	1,24	48,27	39,27	1,39	23,14	52,7	0,78	66	183
MB 107	0,12	0,07	0,14	0,16	0,24	0,25	0,37	0,24	0,30	0,29	0,23	0,29	0,18	0,26	0,19	0,49	0,54	2,89	1,26	31,36	23,55	0,44	33,87	51,7	0,8	62	229

Table 1. Major, minor (Al_2O_3, CaO) and rare earth element and yttrium (REY) contents in the limestones of the Loma Negra Formation, from Sierras Bayas Group. MC: color limestones, MB: black limestones (taken from Gómez-Peral *et al.*, 2019). P (ppm) and S (ppm) are data obtained for the present work.

Sample	Th	Ba	Pb	Cr	Cu	Ni	V	U	V/Cr	V/V+Ni	Th/U	Cr/Th	Y/Ni	EFV	EFU	EFCu	EFNi	Ba/Al
MC 085	5,38	317,94	6,52	9,62	3,64	50,69	4,30	0,23	0,45	0,08	23,78	1,79	0,11	1,27	9,88	1,93	33,60	0,019
MB 087	1,31	485,06	5,58	5,31	36,19	25,31	3,23	0,04	0,61	0,11	36,04	4,04	0,17	1,41	2,36	28,43	24,85	0,051
MB 088	2,40	79,19	3,07	3,15	3,81	7,95	1,44	0,07	0,46	0,15	34,65	1,31	0,64	0,74	5,26	3,51	9,17	0,010
MB 089	1,37	35,72	1,85	1,41	1,30	12,49	0,32	0,04	0,22	0,02	35,44	1,03	0,30	0,13	2,42	0,99	11,83	0,004
MB 091	1,93	69,23	5,60	2,79	4,96	20,62	1,07	0,02	0,38	0,05	112,81	1,44	0,39	0,46	1,09	3,83	19,88	0,009
MB 092	3,92	73,70	5,15	2,11	3,35	18,54	0,75	0,21	0,35	0,04	18,28	0,54	0,45	0,28	12,09	2,29	15,86	0,008
MB 093	2,63	58,97	2,26	1,27	6,70	16,08	1,44	0,10	1,13	0,08	26,55	0,48	0,37	0,58	5,96	4,90	14,70	0,008
MB 094	0,61	58,19	1,80	2,01	3,70	16,75	0,20	0,01	0,10	0,01	50,85	3,30	0,24	0,07	0,64	2,42	13,67	0,006
MB 095	3,42	71,94	3,80	1,55	7,76	15,31	0,73	0,03	0,47	0,05	109,94	0,45	0,51	0,30	1,88	5,68	14,00	0,009
MB 096	0,55	86,45	3,47	8,91	5,86	16,82	0,36	0,03	0,04	0,02	15,83	16,15	0,27	0,14	2,07	4,21	15,12	0,011
MB 097	0,77	56,20	1,27	0,69	1,54	15,03	0,64	0,10	0,93	0,04	7,65	0,89	0,28	0,24	5,52	1,02	12,46	0,007
MB 098	0,32	125,24	2,62	2,50	1,32	16,88	0,31	0,07	0,12	0,02	4,72	7,84	0,27	0,12	3,81	0,91	14,44	0,018
MB 099	0,70	93,71	1,44	0,79	2,85	17,07	0,28	0,00	0,35	0,02	ni	1,13	0,35	0,10	0,01	1,89	14,14	0,012
MB 100	0,54	107,89	1,95	0,23	3,22	15,74	0,25	0,07	1,05	0,02	7,96	0,43	0,34	0,09	3,77	2,17	13,25	0,013
MB 101	1,00	86,32	1,31	0,58	1,32	14,84	0,80	0,01	1,36	0,05	167,31	0,59	0,48	0,29	0,33	0,88	12,30	0,010
MB 102	1,63	176,45	3,13	0,82	3,62	20,01	0,39	0,01	0,48	0,02	173,68	0,50	0,29	0,15	0,54	2,52	17,39	0,021
MB 103	0,67	95,08	1,85	1,72	3,12	15,37	2,29	0,36	1,33	0,13	1,89	2,55	0,53	1,04	23,91	2,54	15,68	0,012
MB 104	1,62	116,19	1,17	0,88	1,95	15,62	0,50	0,01	0,56	0,03	290,36	0,54	0,59	0,22	0,36	1,53	15,34	0,016
MB 105	1,22	108,82	1,83	0,55	2,18	14,77	0,78	0,19	1,43	0,05	6,54	0,45	0,52	0,33	11,62	1,66	13,99	0,012
MB 106	2,21	89,46	2,13	2,23	5,42	18,01	0,72	0,06	0,32	0,04	34,61	1,01	0,50	0,30	3,99	4,11	17,05	0,011
MB 107	0,52	110,89	2,06	0,79	2,40	16,50	0,38	0,04	0,48	0,02	12,66	1,51	0,47	0,17	2,76	1,96	16,83	0,014

Table 2. Trace element concentrations, element ratios and enrichment factors of elemental-geochemical proxies.

geometric average, assuming that the ratio between near neighbour concentrations is constant, as follows: La/La*=LaN [PrN x (PrN/NdN)2], Ce/Ce*=CeN/[Pr x (PrN/NdN)], Eu/Eu*=EuN /(SmNxTb)0.33.

For some interpretations about paleoredox conditions, we use enrichment factors (EF): EF element X=X/Al sample/X/Al average shale (in this case, we choose post-Archean Australian Shale or PAAS values). If EFX is greater than 1, the element X is enriched relative to PAAS. If EFX is lower than 1, it is depleted (Table 2, following Tribovillard *et al.*, 2006; Arrouy and Gómez-Peral, 2021).

The material was housed both in the Centro de Investigaciones Geológicas (CIG-CONICET-UNLP), La Plata, Argentina, and in the Instituto de Hidrología de Llanuras "Dr. Eduardo Usunoff" (IHLLA-CONICET), Azul, Argentina.

MICROTEXTURE AND MAT-RELATED STRUCTURE

Macroscopic description

The basal section of the Loma Negra Formation (~ 8 m thick) is uncomfortably overlaying the shales of the Olavarría Formation (Fig. 2A). This section is composed of abundant to very abundant micritic calcite with scarce to moderate terrigenous components (< 20% of quartz, feldspars, and clay minerals) accompanied by scarce and disseminated organic matter. This section is characterized by reddish or greenish lime-mudstones (MC) with planar or wavy lamination, in some levels show ripples on tops and other levels with cross-lamination (Fig. 2B, C). The middle and upper sections of the unit (~ 33 m thick) are entirely composed of black mudstones (MB), mostly with planar lamination and scarce and rare current ripples on tops recorded exclusively near the transition between the basal and middle sections (Fig. 2D-E). The black limestone is rich in micritic calcite (~90%), with very low terrigenous (~5–10%), and with scarce organic matter content.

In the basal and middle sections of the Loma Negra Formation, mm-scale hemispherical to sub-hemispherical carbonate microstructures were recorded associated with microbialites (Fig. 2F-G). The hemispherical microstructures occur as dozens to more than a hundred forming irregular pavements in the top of limestone beds (Fig. 2F-G). These forms

appear as much as positive and negative epirelief. In positive epirelief, there are hemispherical or roundly elevations, with 0.1 to 0.3 mm high (Fig. 2G). The individuals have diameters ranging from 0.5 mm to 2 mm, while the coalescent microstructures reach diameters of 5 mm to 6 mm (Fig. 2F-G). The individuals are the smallest and more frequent. Nevertheless, the coalescent forms are also common, showing irregularly shaped blisters (Fig. 2F-G).

Microbially induced sedimentary structures, 'MISS', are hardly recognizable on the bed tops when they may appear masked by the hemispherical structures and can be observed in sections perpendicular to lamination. However, apart from the abundant hemispherical microstructures, the limestone presents well developed 'MISS' throughout the entire unit (Fig. 2B). It is possible to recognize small and discontinuous elongate and bifurcated MISS may be related to Kinneyia-Type wrinkle structures (Hagadorn and Bottjer, 1997) represented between ripples (Fig. 2D). In the upper Loma Negra Formation Elephant Skin structures are relatively common at the top of the beds and usually have polygonal or reticulate patterns characterized by pinnacles and reticular ornamentation (Runnegar and Fedonkin, 1992; Gehling, 1999) (Fig. 2H).

Hemispherical microstructures are primarily observed at the top of the hand sample (Fig. 3A). The polished section of a sample rock, perpendicular to lamination, shows that the internal structure consists of alternating clear and dark contorted laminae vertically continuous showing a millimetre-scale (MISS, Fig. 3B). In some sectors of the polished section, it is possible to observe that internal laminae constitute similar morphologies to micro conical stromatolite structures when the pinnacles ridges are well defined, which do not exceed 3 mm high (Fig. 3B, white arrows).

In the top of the hand samples hemispherical to sub-hemispherical irregularly shaped enclosed by MISS dense laminae are observed under loupe magnification (Fig. 3C-D). Elongated pinnacles, show an apparent convex surface with well-defined edges and rounded shapes that are ~ 1 mm in diameter and up to 1 to 2 mm tall, rounded to sub-rounded tops (Fig. 3 C-D).

Microscopic descriptions

The polished perpendicular to lamination sections show microbial mat with micro columnar structures (Fig. 4A-A'). All the samples are composed mainly of micrite and microsparite (Fig. 4B-H). The anastomosing carbonaceous lamination of dark and light crinkled layers are common where the dark layers are usually discontinuous and rich in organic matter (Fig. 4B). Microstylolites are also common in some sections, interpreted as the product of chemical compaction (Fig. 4C). Domal (~ 0.5 mm high) and columnar (~ 2-3 mm high) structures in the organic-rich layers are common (Fig. 4D-E-F). Gas escape-like structures are developed across the micritic limestone cutting and obliterating the primary lamination (Fig. 4 G). These structures are mostly 2–4 mm high and 1–1.5 mm wide. The crestal zone is domed and often has contorted or discontinuous laminae. (Fig. 4 A', G). Micro columnar stromatolite-like structures (Fig. 4A'- F) have conical-domical cross-sections with laminae that vary in thickness. The internal lamination is diffuse, and towards the top of the structure changes from conical to domal (Fig. 4A'- F). Filaments in light layers are sparse and scarce, without evidence of compaction with a good grade of preservation; they are distributed vertically or sub vertically in the micritic limestone (Fig. 4H). The limestone fabrics dominated by compact and opaque organic matter results in no visible filamentous microfossils (Fig. 4E-F).

Under SEM, it is possible to observe the texture of micrite associated with scarce, long and continuous filament-like forms (Fig. 5A). Circular or subcircular empty holes with defined or collapsed edges (~ 20 μm in diameter) may correspond to gas escape-like structures (Fig. 5B). Hemispherical microstructure appears associated with scarce filaments (Fig. 5C-D). Other probable collapse microstructures are recognizable as circular or irregularly shaped (~ 15 μmin diameter) immersed in the micritic microtexture (Fig. 5 E-F).

DETRITAL INPUT, REDOX-SENSITIVE AND GEOCHEMICAL PRODUCTIVITY PROXIES

Geochemical results were grouped regarding the two sedimentary facies: grey, reddish or greenish lime-mudstones with wave and current ripples (MC) and black thin laminated lime-mudstones (MB). REE data presented in Table 1 were obtained previously by Gómez-Peral *et al*. (2019) and are here reconsidered to reinforce the new added geochemical

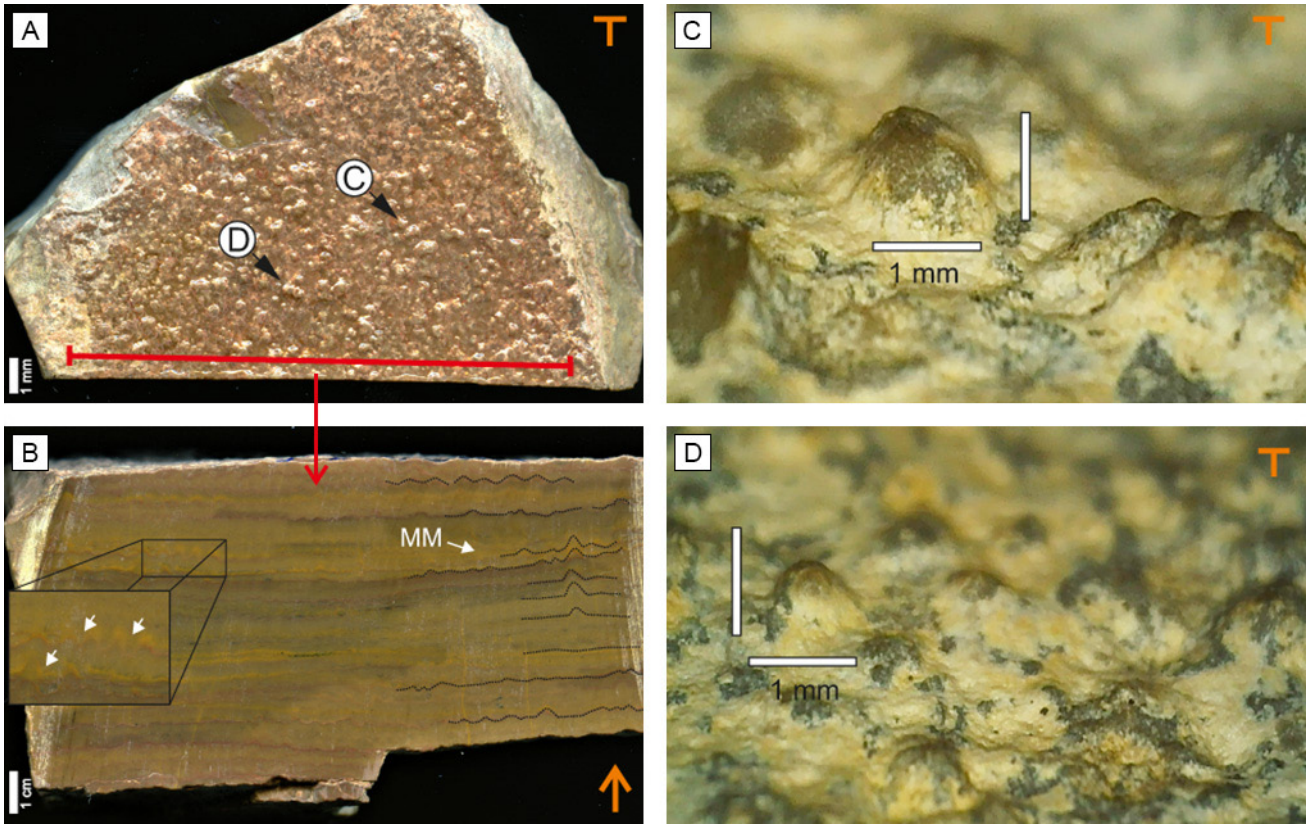

Figure 3. a) The polished perpendicular section shows hemispherical microstructures in top view. **b)** Alternating clear and dark laminae, micro-columnar conical to domal stromatolites (white arrows) associated with microbial mats (MM). **c-d)** Elongated pinnacles.

proxies; as well as Al_2O_3, CaO. On the other hand, S and P values are results obtained from the present work that were included also in Table 1. Added to the later, V, Cr, Co, Ni, Cu, Ba, Pb, Th, U are results also obtained for this contribution (Table 2).

The Al_2O_3, CaO, P, S concentrations and REY results are particularly useful, as they reflect detrital supply, oxygenation conditions, as well as carbonate and biogeochemical productivity (Tribovillard *et al.*, 2006) (Table 1). The average content in$Al_2O_3$is of 2.06% in MC samples and 0.60% in MB samples (Table 1). The CaO, related to carbonate productivity, is 45% on average MC samples and 52% on average MB samples. The P average concentrations are higher (404 ppm in average) in MC samples than in MB samples (89 ppm in average, Table 1).

It is possible to establish similarities and subtle differences from geochemical indicators obtained from MC compared to MB samples. MC values denote a subtle enrichment in light rare earth element compared to the MB average curve (Fig. 6A).

Rare-earth element plus yttrium (REY) abundances in lime-mudstones of the Loma Negra Formation are presented in Table 1 (cf. Gómez-Peral *et al.*, 2019). Total concentrations of REY were 35 ppm on average. The average REY values of the samples represented by MC and MB are compared with the average shale values worldwide (PAAS; Taylor and McLennan, 1985, Fig. 6A).

Ce anomalies (related to other REE; Ce/Ce*) have been used to infer paleo-oceanic redox conditions (Wright *et al.*, 1987; Shields and Stille, 2001). The Ce/Ce* values are in all samples < 1, varying between 0.9 in MC average to 0.6 in MB samples (Table 1; Gómez-Peral *et al.*, 2019). Ce/Ce* can give insight to mainly post-depositional mobility of REE, as Ce/Ce* values are positive (> 1.05) if reducing environmental conditions dominated, and negative (< 0.95) if oxidizing conditions prevailed (e.g. Shields and Stille, 2001; Bau and Dulsky, 1996; Pi *et al.*, 2013). Negative Ce anomalies and positive Y anomalies are related to nearshore and normal seawater conditions (Fig. 6A-C; adapted data from Gómez-Peral *et al.*, 2019). Y/Ho ratios are 32 in average, related to a marine origin (Tostevin *et al.*, 2016; Gómez-Peral *et al.*, 2019). Ce/Ce* values above 0.9 are rare (two MC

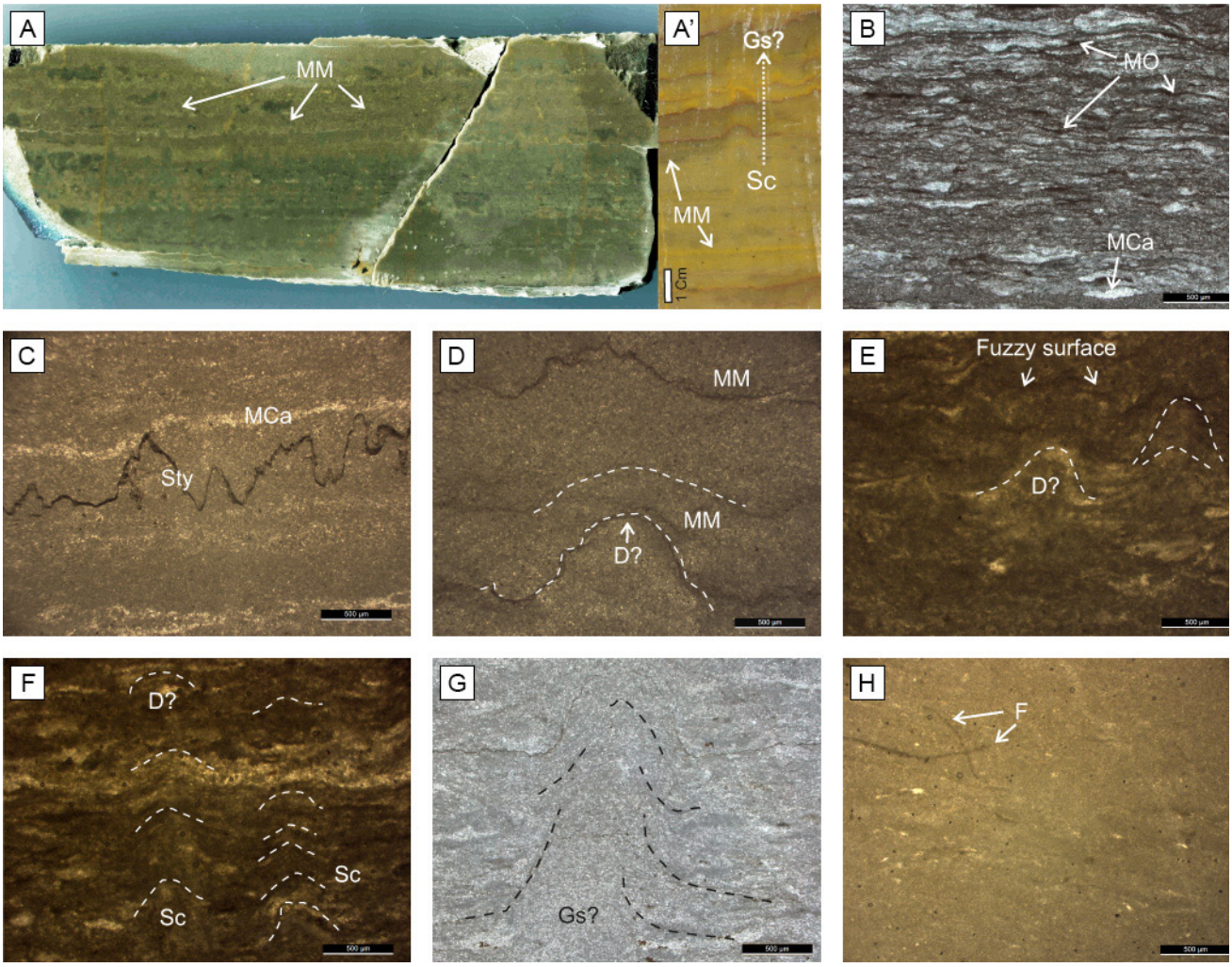

Figure 4. Microphotographs from Loma Negra Formation. **a-a')** polished perpendicular sections show microbial mat (MM), micro columnar structures (Sc) and gas escape-like structures (Gs). **b)** Carbonaceous lamination of dark (rich in organic matter: OM) and light recrystallized microsparite (MCa). **c)** Microstylolites (Sty). **d-e-f)** Domal (D) and columnar structure(Sc) and microbial mats (MM). **g)** Gas escape-like structures (Gs). **h)** Filaments (F) in the micritic limestone.

samples), and they show a definite trend to lower values (Fig. 6B-C; cf. Gómez-Peral *et al.*, 2019). The Ce depletion in sea water depends on the oxidation potential (German and Ederfield, 1990), but also on microbial activity that catalyses the oxidation of Ce^{+3} and controls the pH of pore fluids (Stille *et al.*, 2000). Moreover, any Ce anomaly is likely to reflect the redox and pH paleoenvironmental conditions and, more importantly, those conditions may be preserved during diagenesis (Shields and Stille, 2001). Results important to consider that Ce anomaly represent primary signature if no correlation with LaN/SmN is observed and when LaN/SmN ratios > 0.35 (McArthur and Walsh, 1984; Shields and Stille, 2001; Morad and Felitsyn, 2001). Studied samples, with three exceptions, fulfil this requirement (Table 1, Fig. 6B; cf. Gómez-Peral *et al.*, 2019), and their composition may reflect the paleoseawater redox conditions (Bau and Dulski, 1996; Shields and Stille, 2001; Gómez-Peral *et al.*, 2014; 2019; Arrouy and Gómez-Peral, 2021). La-anomaly may affect the Ce/Ce* causing apparent anomalies, Bau *et al.* (1996) proposed to check La anomalies using Pr/Pr* = 2PrN/(CeN + NdN).

Abundances in some selected trace elements (V, Cr, Ni, Cr, Cu, Pb, Th, U, Ba) from the Loma Negra mudstones were determined and listed in Table 2. Some of these element concentrations in bulk samples are probably mixtures of both detrital and authigenic components that vary in response to redox conditions in the water column (Pi *et al.*, 2011).

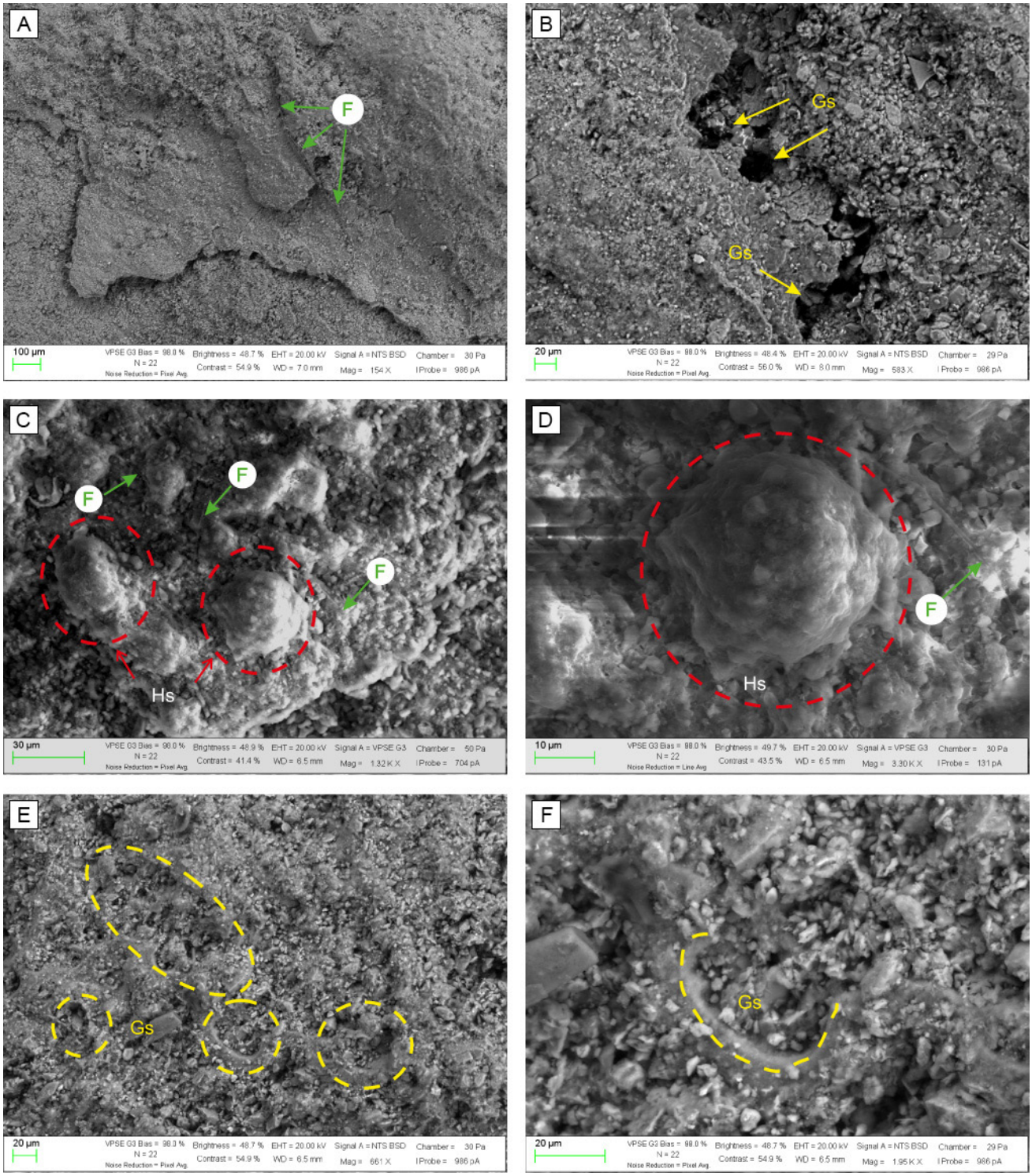

Figure 5. SEM-EDAX microphotographs. a) nanofilaments (F) in micritic microtexture. b) Circular or subcircular empty holes, (gas escape-like structures - Gs). c-d) Hemispherical microstructures (red circle - Hs) associated with filaments. e-f) collapsed microstructures immerse in the micritic microtexture.

The samples show concentrations of Pb, Cr and Cu with values of 2.85, 2.37 and 3.5 on average, respectively. One sample, MB 087, shows a higher value of Cu of 36 ppm. Ratios of Th/U are 58.6, Cr/Th of 2.3, Y/Ni of 0.39 on average, respectively (Table 2).

The redox-sensitive trace elements U, V, and Ni (Tribovillard *et al.*, 2006; Pi *et al.*, 2013; Arrouy and Gómez-Peral, 2021) show almost no variation with

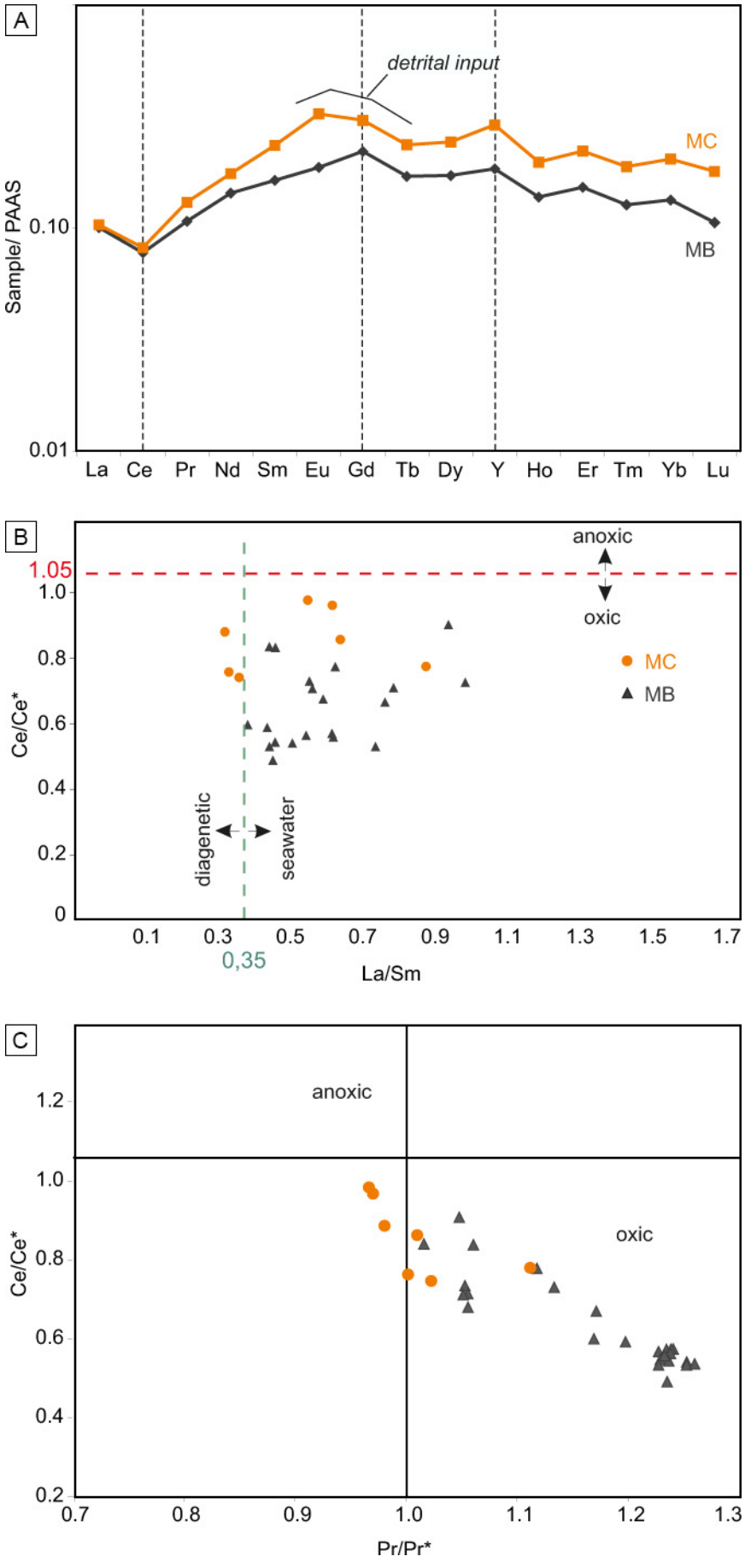

Figure 6. a) Shale-normalized (PAAS) average REY patterns of carbonates from reddish limestones (MC in orange) and black limestones (MB in black). **b)** Relationship diagram of Ce/Ce* vs La/Sm. **c)** Ce/Ce* vs. Pr/Pr* after Lawrence and Kamber, 2006 (modified from Bau and Dulski, 1996).

average contents of 0.08 ppm, 1 ppm and 18.1 ppm, respectively.

The V/(V +Ni) values, used as a redox paleoproxy (Arthur and Sageman, 1994), are uniformly low (0.05 in average, Table 2) and V/Cr < 2 are extremely low in the limestones of Loma Negra Formation (0.6 in average, Table 2).

To make results easier to interpret, it is common to use enrichment factors (EF): EF element X=X/Al sample/X/Al average shale. If EFX is greater than 1, then element X is enriched relative to average shales and, if EFX is less than 1, it is depleted. Table 2 gives values of enrichment factors of V, U, Cu and Ni.

VEF values are lower than 2 in all analyzed samples (0.4 on average). UEF is 4.8 on average, while three samples show values > 10. CuEF is 3.8 (2 samples show values > 5), and NiEF is 16.1 on average, and Ba/Al is 0.013 on average (Table 2).

Figure 7A and 7B is used to indicate oxygenated conditions throughout the succession which seem to be maintained through time with the exception of one sample from the base of MC. P ppm values, related to organic productivity, show an absence of correlation with Ni (ppm) or VEF, both considered as paleoredox proxies (Fig. 7C-D). Positive correlations between S (ppm) with Ni (ppm) or with VEF indicate an increment in H_2S activity related to relatively less oxygenated seawaters (Fig. 7 E-F). UEF, as redox proxy, is compared to V/Cr and VEF, respectively (Fig. 7 G-H).

DISCUSSION

Paleoenvironmental conditions - Background

The Ediacaran Loma Negra Formation was defined as a unit composed entirely of lime mudstones deposited in a platform environment related to the Clymene Ocean in the Southwestern part of Gondwana (Gómez-Peral *et al*., 2018; 2019). This extense carbonate platform, was divided by those authors into two sedimentary facies, the basal section, reddish or greenish limestones, and the middle and upper sections conformed by black limestones, in which lime mud originated by suspension fall-out in an open-marine ramp. The limestones revealed constant positive $\delta^{13}C$ curves, similar to those recorded in other middle-Ediacaran marine records worldwide. The retained original fabric of micritic limestones represent unusual preservation of isotope compositions, considering the geochemical multi-proxies (Gómez-Peral *et al*., 2018). Added to the micrite, the organic matter appears disseminated between the laminae of these microbial mats (Fig. 4B). This organic matter was previously analyzed by Gómez-Peral *et al*. (2007), who indicated a high degree of preservation.

The Loma Negra limestones had been accumulated shallow middle to outer ramp environment under low-moderate to low energy conditions (Gómez-Peral *et al*., 2019), creating the necessary environmental conditions for the microbial mats development and growth described. Velazquez-Bagnaud *et al*. (2013) pointed out that the recognition of specific biomarkers in the microbialites of the Loma Negra Formation indicated the activity of diverse microbial communities, including primary producers such as cyanobacteria, phototrophic bacteria, green bacteria and some methanogenic bacteria. From the present work, the detailed meso-, micro- and submicroscopic characterization suggest that the entire Loma Negra Formation, a carbonate sequence, was produced by the biological influence with trapping sedimentary particles and precipitation in situ of carbonate.

Microbialites

The well-preserved primary lamination interlayered with organic matter recorded throughout the complete Loma Negra Formation can be associated with microbial activity (Figs. 2A, 3B and 4B). As was explained by Nofke and Awramik 2013, it is essential to consider that the repetitive precipitation of carbonates in extracellular polymeric together with sediment trapping and binding substances causes stromatolite buildups within carbonate deposits. The thin-sections descriptions allow us to recognize the presence of 'MISS' represented by microtextures related to ancient biofilms or microbial mats.

The most common 'MISS' found in the Loma Negra formation could be attributed to the Kinneyia-style wrinkle structures (Hagadorn&Bottjer, 1997; Schieber, 1998, 1999, Porada and Bouougri 2007). Kinneyia-style may develop where microbes settle on a sediment surface and eventually form a cohesive mat. These zones consist of water saturated sediment and organic material, originating mainly from heterotrophs and their mucilage (Fenchel and Kühl, 2000).

Elephant Skin structures are also relatively

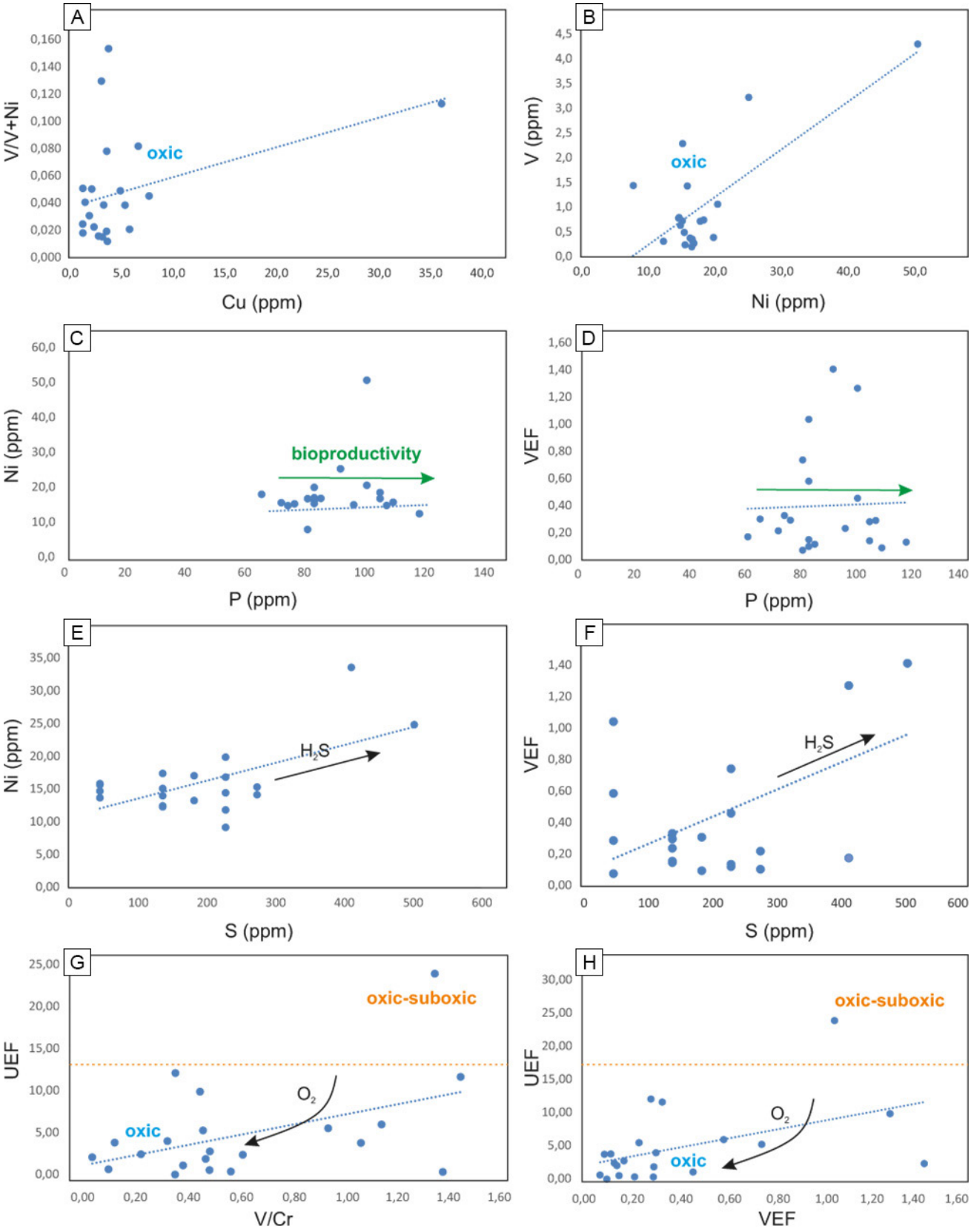

Figure 7. a) V/V+Ni vs Cu (ppm) diagram. **b)** V(ppm) vs Ni(ppm) diagram. **c-d)** P (ppm) vs Ni and P (ppm) vs VEF diagrams. **e-f)** S (ppm) vs Ni (ppm) and S vs VEF diagrams. **g-h)** UEF vs Cu (ppm) and UEF vs VEF diagrams.

common at the top of the sequence and are characterized by cracked, varying from tufts, pinnacles and pustules to bulges and reticulate ornamentation (cf. 'Elephant skin'; Gehling, 1999) (Fig. 2H).

The record of stromatolites in carbonate rocks is assumed as developed from the microbial mat accumulated (Semikhatov *et al.*, 1979). The micro-stromatolites represented in the Loma Negra Formation are associated with the microbial mat showing micro-columnar conical to domical structures (Fig. 4A'- F) having cross-sections with laminae that vary in thickness.

The growth model for Loma Negra micro-stromatolites indicated that the behaviour and distribution of microbial communities dominated the morphological evolution of micro-columnar conical to domal stromatolites, also morphologically similar to the pinnacles described by Sumer *et al.* (2016). According to these authors, those pinnacles grew in an environment with sufficient light and low sedimentation rate.

Microbial mats with preserved filaments have been known since the Proterozoic, and well preserved examples were recorded in Mesoproterozoic limestones from the North of China (Zhao *et al.*, 2020). Sparsely represented filaments in the Loma Negra Formation were observed associated with the microbial mats represented by scarce intertwined or interlaced filaments (Fig. 4H; Fig. 5A, C).

Photosynthesis as bubble producer

Microbialites related to oxygenic photosynthesis have been studied with great detail in modern cyanobacteria-dominated microbial mats (Jorgensen *et al.*, 1983; Bosak *et al.*, 2009, 2010; Sim *et al.*, 2012;). The morphology of mats can further preserve physiological indicators, including the production and subsequent trapping of gas bubbles from oxygenic photosynthesis (Bosak *et al.*, 2009, 2010).

The gases, uprising from buried and decaying organic matter, tend to accumulate beneath the strongly cohesive mats covering the sediment surface, which inhibits gas escape to the exterior and accumulates in the pore spaces of the sediment and between the organic colonies. (see e.g., Reineck *et al.*, 1990; Noffke *et al.*, 1996; Gerdes *et al.*, 2000). With increasing gas pressure, grains and the organic components may be pushed, resulting in the formation of hemispherical structures like cavities (Gerdes *et al.*, 2000) and, in extreme cases, as in the basal and middle Loma Negra Formation, developing a sponge pore texture of the sediment.

The recognition of gas-related morphologies in fossil microbialites requires that bubbles form and remain attached to the mat and that the mat around them be preserved by lithification (Bosak *et al.*, 2010). These bubbles-like structures may be represented in the Loma Negra Formation by the detailed described hemispherical microstructures (Figs. 2F-G; 3A, C, D) interpreted from their macro and micro features as being associated with the microbial mat gas production and gas scape (Fig. 4A', G; and 5B, E, F). These microbially coated bubbles can be filled later with sediments and therefore have the potential of preservation in sediments (Fig. 3A; 5C-E). The recognition of fossil bubbles-like structures as features with nearly-spherical cross-sections will be possible if sufficiently small crystals preserve the surrounding microbial mesh and without significant recrystallization (Bosak, 2009; Gómez-Peral *et al.*, 2018; 2019).

Due to the sealing of impermeable mats on the sediment surface, the escaping gas will push the mat upwards to form various bubbles-like structures observed in Fig. 3A. These structures were also recognized in other Precambrian successions (Noffke *et al.*, 2000; Eriksson *et al.*, 2007; Sarkar *et al.*, 2008).

The depth distribution of the hemispherical microstructures in the studied lithofacies is controlled by bubble nucleation, which depends on hydrostatic pressure, dissolved gas concentration, and flux of gasses within mats (Bosak *et al.*, 2010). Preservation of bubbles within mats requires rapid lithification (e.g., Chafetz *et al.*, 1991), and early carbonate precipitation likely lithified the buoyed mat to provide a substratum for subsequent micro-stromatolitic growth (Fig. 3B). The paleoenvironmental evolution of the depositional setting in the carbonate ramp of the Loma Negra Formation was indicated as deepening upwards the succession (Gómez-Peral *et al.*, 2019). This progressive relative sea-level rise may inhibit the bubble nucleation due to increased hydrostatic pressure and less gas supersaturation within microbial mats. The analyzed samples revealed a sedimentary succession with the most concentrated gas scape and bubbles-like structures recorded in the lower and middle sections compared to the upper

section of the unit (where are almost absent).

Oxygenation proxies

A more continuous knowledge into the Precambrian, particularly into the Ediacaran seawater redox conditions, is needed to better constrain Ediacaran oxygenation's influence over biological evolution (Shields-Zhou and Och, 2011; Gómez-Peral *et al*., 2019).

Microbial and non-skeletal carbonate may supply a more certain proxy for seawater REY concentrations than skeletal carbonate (Webb and Kamber, 2000). The REY behaviour in Precambrian marine limestones was recently investigated (Frimmel, 2009; Zhao *et al*., 2009; Ling *et al*., 2013; Wei *et al*., 2018; 2019).

The Al_2O_3, CaO, P, S concentrations and REY were analyzed to reflect variations in detrital supply, oxygenation conditions, carbonate, and biogeochemical productivity (Tribovillard *et al*., 2006; Gómez-Peral., 2019; Table 1). The Al_2O_3 average content is higher in the basal than in the middle and upper sections (Table 1). This variation is attributed to the relatively higher terrigenous supply in the basal section. The P concentration related to bioproductivity is higher in the upper section than in the lower section (Fig. 7C-D). In addition, a subtle enrichment in light rare earth element, REY, upwards the unit is associated with the decrease in the detrital input for the rise in carbonate productivity. This detrital contribution decrease meant to respond to the turn from the nearshore to open marine deposits.

Negative Ce anomalies in calcite microbialites may be a strong indicator of oxic conditions of the primary water body. Positive anomalies are more likely to be diagnostic of suboxic to anoxic diagenetic conditions (Holser, 1997; Laenen *et al*., 1997). The limestones of the Loma Negra Formation show a record of negative Ce anomalies varying from 0.49 to 0.98 (Fig. 6B-C, Table 1).

The high Th/U values indicate the influence of detrital components and also oxic conditions in the environmental setting. The redox-sensitive trace elements U, V, and Ni (Tribovillard *et al*., 2006; Pi *et al*., 2013; Arrouy and Gómez-Peral, 2021) show almost no variation with average contents. The V/(V +Ni) values, used as a redox paleoproxy (Arthur and Sageman, 1994), are uniformly low (Table 2), suggesting a deposition under oxic conditions. V/Cr < 2 are extremely low (Table 2), supporting the interpretation of oxygenated conditions at the seawater sediment interface (Arthur and Sageman, 1994).

Redox-sensitives of the analyzed samples indicate well- and maintained- high oxygenated conditions throughout the entire succession, with one sample from the base of the unit related to relatively lower oxygenated conditions. The extensive marine connection of the interior seas and the marginal and oceanic basins, known as the Clymene Ocean (Warren *et al*., 2014), provided the ideal conditions for the deposition of shallow carbonate facies with microbialites. In this context, the oxygenation proxies recorded in the Loma Negra Formation allows us to speculate that process from cyanobacteria-dominated microbial mats could have produced the rise in oxygen during accumulation (Bosak *et al*., 2009, 2010). This reinforces the idea of the connected and well oxygenated (non-stratified) sea during the accumulation of these limestones.

According to that postulated by Gómez-Peral *et al*. (2019), the Loma Negra Formation sustain evidence of the middle Ediacaran Oceanic Oxygenation Event in this southwestern Gondwana setting (OOE: ca. 580 Ma, Sahoo *et al*., 2016). The occurrence of this OOE in an anoxic context could be explained by an intense photosynthetic microbial activity in this epeiric sea recorded throughout the extensive carbonate platform represented by the Loma Negra Formation.

FINAL REMARKS

The Loma Negra limestones were accumulated in a well-oxygenated shallow ramp under low energy conditions providing the necessary environmental requirements to the sustained microbial activity.

The well-preserved primary lamination interlayered with organic matter recorded throughout the entire unit is interpreted as produced by microbial mats with scarce preservation of filaments. Two kinds of MISS are recognized in the Loma Negra Formation; one resembles the Kinneyia-style micro wrinkles and the other the Elephant skin.

The detailed characterization of micro-columnar conical to domical stromatolites associated with microbial mats was conducted first in the present work.

Abundant bubbles-like and gas escape structures

associated with the microbial mats recovered from the bed-tops of the lower and middle sections of the Loma Negra Formation might be interpreted as the result of gas trapping beneath the mat. The morphology of bubbles-like structure is comparable with the oxygen bubbles produced in the laboratory by modern cyanobacteria-dominated microbial mat as the manifestation of photosynthetic oxygen production.

The evolution in the depositional settings of the unit was indicated as deepening upwards. The related sea-level rise may inhibit the bubble nucleation in response to increased hydrostatic pressure. That could be evidenced by the higher concentration of gas scape and bubbles-like structures in the basal and middle sections than in the upper succession.

The rise in oxygen, related to the previously reported middle Ediacaran Oceanic Oxygenation Event in the Loma Negra Formation, could be associated with the intense photosynthetic oxygen production by the microbial activity.

Acknowledgements

We wish to extend our gratitude to the Cementos Avellaneda S.A. for logistic support in the field. Fieldwork and laboratory materials were supported by grants to MJA and LGP (PICT 2017-0747; PICT 2018-4022 and UNLP-PID N888). Prof. Claudia Cavarozzi is thanked for the ICP-MS analysis, and Pablo Garcia for the preparation of polished and thin sections. Prof. Lucas Warren is especially thanked for the logistics in SEM-EDS in UNESP- Brazil. We especially thank to the reviewer, Dr Ricardo Jahnert, and the editors from the present special volume, Dr Fernando Gomez and Dr Anelize Bahniuk, for their comprehensive and detailed evaluation of the original manuscript improving the present version.

REFERENCES

Arrouy, M. J., Poiré, D. G., Gómez-Peral, L. E., and Canalicchio, J. M. (2015). Sedimentología y estratigrafía del Grupo La Providencia (Nom. Nov.): Cubierta Neoproterozoica, Sistema de Tandilia, Argentina. *Latin American Journal of Sedimentology and Basin Analysis* 22 (2), 1–38.

Arrouy, M.J., Warren, L.V., Quaglio, F. Poiré, D.G., GuimarãesSimões, M., Boselli, M.R., and Gómez-Peral, L.E. (2016). Ediacaran discs from South America: probable soft-bodied macrofossils unlock the paleogeography of the Clymene Ocean. *Scientific Reports,* 6:30590, 1-10. DOI: 10.1038/srep30590.

Arrouy, M.J., and Gómez-Peral, L.E. (2021). Exposing the inside of the fine-grained siliciclastic tidal shelf deposits of the Alicia Formation, Tandilia Basin, during the Ediacaran anoxia in the Clymene Ocean. *Journal of South American Earth Sciences*, 102945. https://doi.org/10.1016/j.jsames.2020.102945.

Arthur, M.A., and Sageman, B.B. (1994). Marine black shales. Depositional and mechanisms and environment of ancient deposits. *Annual Review of Earth and Planetary Sciences*, 22:499–551.

Bagnoud-Velásquez, M., Spangenberg, J.E., Poiré, D.G., and Gómez-Peral, L.E., (2013). Stable isotope (S, C) chemostratigraphy and hydrocarbon biomarkers in the Ediacaran upper section of Sierras Bayas Group, Argentina. *Precambrian Research*, 231:388-400.

Banerjee, S., Sarkar, S., and Eriksson, P.G. (2014). Palaeoenvironmental and biostratigraphic implications of microbialmat-related structures: examples from modern Gulf of Cambay and Precambrian Vindhyan basin. *Journal of Palaeogeography* 3(2), 127-144.

Bau, M., and Dulski, P. (1996). Distribution of yttrium and rare-earth elements in the Penge and Kuruman iron-formations, Transvaal Supergroup, South Africa. *Precambrian Research* 79 (1–2):37–55. https://doi.org/10.1016/0301-9268(95)00087-9.

Bosak, T., Liang, B., Sim, M.S., and Petroff A.P. (2009). Morphological record of oxygenic photosynthesis in conical stromatolites. *Proceedings of the National Academy of Sciences*. USA 106:10939–43.

Bosak, T., Bush, J.W.M., Flynn, M., Liang, B., Ono, S., Petroff, A.P., and Sim, M.S. (2010). Formation and stability of oxygen-rich bubbles that shape photosynthetic mats. *Geobiology,* 8:45–55.

Chafetz H.S., Rush P.F. and Utech N.M., (1991) Microenvironmental controls on mineralogy and habit of CaCO3 precipitates: an example from an active travertine system. *Sedimentology,* 38:107–126.

Chen, Z., Zhou, C., Meyer, M., Xiang, K., Schiffbauer, J. D., Yuan, X., and Xiao, S. (2013). Trace fossil evidence for Ediacaran bilaterian animals with complex behaviors. *Precambrian Research*, 224:690–701.

Cingolani, C. (2011). The Tandilia System of Argentina as a southern extension of the Río de la Plata craton: an overview. *International Journal of Earth Sciences* 100:221–242.

Cui, H., Kaufman, A.J., Xiao, S., Zhu, M., Zhou, C., and Liu, X-M. (2015). Redox architecture of an Ediacaran ocean margin: integrated chemostratigraphic (d13C–d34S–87Sr/86Sr–Ce/Ce*) correlation of the Doushantuo Formation, South China. *ChemicalGeology*, 405:48–62.

Dalla Salda, L. and Iñiguez Rodríguez, A.M. (1979). *La Tinta, Precámbrico y Paleozoico de Buenos Aires*. VII Congreso Geológico Argentino, Buenos Aires. Actas I: 539–550.

Eriksson, P.G., Simpson, E.L., Eriksson, K.A., Bumby, A.J., Steyn, G.L., and Sarkar, S. (2000). Muddy roll-up structures in siliciclastic interdune beds of the ca. 1.8 Ga Waterberg Group, South Africa.*Palaios,* 15: 177–183.

Eriksson, P. G., Sarkar, S., Banerjee, S., Porada, H., Catuneanu, O., and Samanta, P. (2010). Paleoenvironmental context of microbial mat-related structures in siliciclastic rocks: Examples from the Proterozoic of India and South Africa; In: Microbial mats: Modern and ancient microorganisms in stratified systems (eds) Seckbach J and Oren A, Springer-Verlag, Berlin, pp. 73–108.

Fenchel, T. and Kühl, M. (2000) Artificial cyanobacterial mats: growth, structure, and verticalzonation patterns. Microb. Ecol. 40, 85-93.

Gehling, J.G. (1999). Microbial mats in terminal Proterozoic siliciclastics: Ediacaran death masks. *Palaios* 14: 40–57.

Gerdes, G., Klenke, T., and Noffke, N. (2000). Microbial signatures in peritidal siliciclastic sediments: a catalogue. *Sedimentology* 47: 279–308.

German, C.R., Elderfield, H., 1990. Application of the Ce anomaly as paleoredox indicator: the ground rules. Paleoceanography 5, 823–833.

Gómez-Peral, L.E., D.G. Poiré, H. Strauss H., and Zimmermann, U. (2007). Chemostratigraphy and diagenetic constraints on Neoproterozoic carbonate successions from the Sierras Bayas Group, Tandilia System, Argentina. *Chemical Geology* 237, 127–146.

Gómez-Peral, L.E., Raigemborn, M.S., and Poiré, D.G. (2011). Petrología y evolución diagenética de las facies silicoclásticas del Grupo Sierras Bayas, Sistema de Tandilia, Argentina. *Latin American Journal of Sedimentology and Basin Analysis* 18 (1), 3–41.

Gómez-Peral, L.E., Kaufman, A.J., and Poiré, D.G. (2014). Paleoenvironmental implications of two phosphogenic events in Neoproterozoic sedimentary successions of the Tandilia System, Argentina. *Precambrian Research*, 252, 88–106.

Gómez-Peral, L.E., Sial, A.N., Arrouy, M.J., Richiano, S., Ferreira, V.P., Kaufman, A.J., and Poiré, D.G. (2017). Paleoclimatic and paleoenvironmental evolution of the Early Neoproterozoic basal dolomitic platform, Río de La Plata Craton, Argentina: insights from the $\delta^{13}C$ chemostratigraphy. *Sedimentary Geology*, 353: 139–157.

Gómez-Peral, L.E., Kaufman, A.J., Arrouy, M.J., Richiano, S., Sial, A.N., Póiré, D.G., and Ferreira, V.P. (2018). Preglacialpalaeoenvironmental evolution of the Ediacaran Loma Negra Formation, far southwestern Gondwana, Argentina. *Precambrian Research*, 315: 120–137. https://doi.org/10.1016/j.precamres.2018.07.00.

Gómez-Peral, L.E., Arouty, M.J., Poiré, D.G., and Cavarozzi, C.E. (2019). Redox-sensitive 803 element distribution in the Neoproterozoic Loma Negra Formation in Argentina, in 804 the Clymene Ocean context. *Precambrian Research*, 332: 105–384. https://doi.org/10.1016/j.precamres.2019.105384.

Gómez-Peral, L.E., Arouy, M.J., Richiano, S., Cereceda, A. Alé, S.A., and Poiré, D.G. (2021). Unravelling hidden glacial effects in the Cryogenian marine depositional settings of the Tandilia Basin, Argentina. *Precambrian Research*, 106261. https://doi.org/10.1016/j.precamres.2021.106261.

Hagadorn, J.W., and Bottjer, D.J. (1997). Wrinkle structures: Microbially mediated sedimentary structures common in subtidal siliciclastic settings at the Proterozoic-Phanerozoic transition: Geology, v. 25, p. 1047-1050.

Halverson, G.P., Hoffman, P.F., Schrag, D.P., Maloof, A.C., and Rice, A.H.N. (2005), Toward a Neoproterozoic composite carbon-isotope record: *Geological Society of America Bulletin*, v. 117, (9): 1181–1207.

Hartmann, L.A., Santos, J.O.S., Bossi, J., Campal, N., Schipilov, A., and McNaughton, N.J. (2002). Zircon and titanite U-Pb SHRIMP geochronology of Neoproterozoic felsic magmatism on the eastern border of the Rio de la Plata Craton, Uruguay. *Journal of South American Earth Sciences* 15: 229–236.

Hernández, M., Arrouy, M.J., Scivetti, N., Franzese, J.R., Canalicchio, J.M., and Poiré, D.G. (2017). Tectonic evolution of the Neoproterozoic Tandilia Sedimentary cover, Argentina: new evidence of contraction and extensional events in the southwest Gondwana margin. *Journal of South American Earth Sciences* 79: 230–238.

Homann, M.; Heubeck, C., Airo, A., and Tice, M. M., (2015) Morphological adaptations of 3.22 Ga-old tufted microbial mats to Archean coastal habitats (Moodies Group, Barberton Greenstone Belt, South Africa), *Precambrian Research*, Vol. 266, 47-64, https://doi.org/10.1016/j.precamres.2015.04.018.

Holser, W.T. (1997). Evaluation of the application of rare-earth elements to paleoceanography. *Palaeogeography Palaeoclimatolology Palaeoecology* 132, 309–323.

Iñiguez Rodríguez, A. M. (1999). La Cobertura Sedimentaria de Tandilia. In: Caminos R. (Ed), Geología Argentina. (SEGEMAR). pp 101–106.

Jorgensen B.B., Revsbech N.P., and Cohen Y. (1983). Photosynthesis and structure of benthic microbial mats: microelectrode and SEM studies of four cyanobacterial communities. *Limnology and Oceanography* 28, 1075–1093.

Laenen, B., Hertogen, J., and Vandenbarghe, N. (1997). The variation of the trace-element content of the fossil biogenic apatite through eustatic sea level cycles. *Paleogeography Paleoclimatology Paleoceanography* 132, 325-342.

Ling, H.F., Chen, X., Li, D., Wang, D., Shields-Zhou, G.A., and Zhu, M. (2013). Cerium anomaly variations in Ediacaran-earliest Cambrian carbonates from the Yangtze Gorges area, South China: implications for oxygenation of coeval shallow seawater. *Precambrian Research* 225, 110–127.

Luo M, Chen Z, Hu S, Zhang Q, Benton M J, Zhou C, Wen W and Huang J. (2013). Carbonate reticulated ridge structures from the lower middle Triassic of the Luoping Area, Yunnan, southwestern China: Geobiologic features and implications for exceptional preservation of the Luoping Biota; *Palaios* 28 541–551.

Lyons, T.W., Reinhard, C.T., and Planavsky, N.J. (2014). The rise of oxygen in Earth/'s early ocean and atmosphere. *Nature* 506, 307–315

Macdonald, F.A., Jones, D.S., and Schrag, D.P. (2009). Stratigraphic and tectonic implications of a newly discovered glacial diamictite–cap carbonate couplet in southwestern Mongolia. *Geology* 37 (2), 123-126.

Mata, S.A., Harwood, C.L., Corsetti, F.A., Stork, N.J., Eilers, K., Berelson, W.M., and Spear, J.R. (2012). Influence of gas production and filament orientation on stromatolite
microfabric. *Palaios* 27, 206–219.

Marchese H.G., and Di Paola E. (1975). Miogeosinclinal Tandil. *Revista de la Asociación Geológica Argentina* 30(2):161–179.

McArthur, J.M., and Walsh, J.N. (1984). Rare-earth element geochemistry of the phosphorites. *Chemical Geology* 47, 191–220.

McLennan, S.M. (1989). Rare earth elements in sedimentary rocks: influence of provenance and sedimentary processes. In: Lipin, B.R., McKay, G.A. (Eds.), Geochemistry and Mineralogy of Rare Earth Elements. Min. Soc. Am. Rev. Mineral., vol. 21, pp. 169–200.

Morad, S., and Felitsyn, S. (2001). Identification of primary Ce-anomaly signatures in fossil biogenic apatite: implication for the Cambrian oceanic anoxia and phosphogenesis. *SedimentaryGeology* 143, 259–264.

Nágera, J.J. (1940). Tandilia. Biblioteca Facultad de Ciencias Naturales y Museo, Universidad Nacional de La Plata XXIV. pp. 272.

Noffke N., Gerdes, G., Klenke, T., and Krumbein W.E. (1996). Microbially induced sedimentary structures – examples from modern sediments of siliciclastic tidal flats.

ZentralblattGeologie und Paläontologie, 1:307–316.

Noffke, N., Gerdes, G., Klenke, T., and Krumbein, W.E. (2001). Microbially induced sedimentary structures a new category within the classification of primary sedimentary structures. *Journal of Sedimentary Research*, 71, 649–656.

Noffke, N., Gerdes, G., and Klenke, T. (2003). Benthic cyanobacteria and their influence on the sedimentary dynamics of peritidal depositional systems (siliciclastic, evaporitic salty, and evaporitic carbonatic). *Earth-Science Reviews* 62, 163–176.

Noffke, N., Christian, D., Wacey, D., and Hazen, R.M. (2013). Microbially induced sedimentary structures recording an ancient ecosystem in the ca. 3.48 billion-year-old Dresser Formation, Pilbara, Western Australia. *Astrobiology* 13, 1103–1124.

Och, L.M., and Shields-Zhou, G.A. (2012). The Neoproterozoic oxygenation event: environmental perturbations and biogeochemical cycling. *Earth-Science Reviews,* 110:26–57.

Pankhurst, R.J., Ramos, A., and Linares, E. (2003). Antiquity of the Río de la Plata craton in Tandilia, southern Buenos Aires province, Argentina. *Journal of South American Earth Sciences,* 16:5–13.

Pi, D. H., Liu, C. O., Shields-Zhou, G.A., and Jiang, S. Y. (2013). Trace and rare earth element geochemistry of black shale and kerogen in the early Cambrian Niutitang Formation in Guizhou province, South China: constraints for redox environments and origin of metal enrichments. *PrecambrianResearch*, 225:218–229.

Poiré, D.G., González, P.D., Canalicchio, J.M., and García Repetto, F. (2005). Estratigrafía del Grupo Mina Verdún, Proterozoico, Uruguay. *Latin American Journal of Sedimentology and BasinAnalysis,* 12:125–143.

Poiré, D.G., Gómez-Peral, L.E., and Arrouy, M.J. (2018). Glaciations in South America. In: Geology of Southwest Gondwana, Siegesmund, S., Basei, M.A.S., Oyhantçabal, P., Oriolo, S. (Eds.). Special Publication of Springer Nature, 527-541. https://doi.org/10.1007/978-3-319-68920-3_19.

Porada, H., and Bouougri, E. (2007). "Wrinkle structures" da critical review. In: Schieber, J., Bose, P.K., Eriksson, P.G., Banerjee, S., Sarkar, S., Altermann, W., Catuneanu, O. (Eds.), Atlas of Microbial Mat Features Preserved Within the Siliciclastic Rock Record. Elsevier, Amsterdam, pp. 135-144.

Reinech,H.E., Gerdes, G., Claes, M., Dunajtschik, K., Riege, H., and Krumbein, W.E. (1990). Microbial modification of sedimentary surface structures, in Heling, D., Rothe, P., Förstner, U., and Stoffers, P., eds., Sediments and Environmental Geochemistry: Springer-Verlag, Berlin, p.254–276.

Runnegar, B., and Fedonkin, M. (1992). Proterozoic metazoan body fossils. In: Schopf, J., Klein, C. (Eds.), The Proterozoic Biosphere, A Multidisciplinary Study. Cambridge Univ. Press.

Sahoo, S.K., Planavsky, N.J, Kendall, B., Wang, X., Shi, X., Scott, C., Anbar, A.D., Lyons, T.W., and Jiang G. (2012). Ocean oxygenation in the wake of the Marinoan glaciation. *Nature,* 489:546–549.

Sahoo, S. K., Planavsky, N.J., Jiang, G., Kendall, B., Owens, J.D., Wang, X., Shi, X., Anbar, A.D., and Yons, T.W.L. (2016). Oceanic oxygenation events in the anoxic Ediacaran ocean. *Geobiology,* 14:457–468.

Sallstedt, T., Bengtson, S., Broman, C., Crill, P.M., and Canfield, D.E. (2018). Evidence of oxygenic phototrophy in ancient phosphatic stromatolites from the Paleoproterozoic Vindhyan and Aravalli Supergroups, India. *Geobiology,* 16:139–159.

Sarkar, S., Choudhuri, A., Banerjee, S., Van Loon, A. J., and Bose, P. K. (2014a). Seismic and non-seismic soft sediment deformation structures in the Proterozoic Bhander Limestone, central India; *Geologos,* 20:89–103.

Sarkar, S., Choudhuri, A., Mandal, S., and Eriksson, P.G. (2016). Microbial mat-related structures shared by both siliciclastic and carbonate formation; *Journal of Palaeogeography,* 5:278–291.

Schieber, J., Bose, P. K., Eriksson, P. G., Banerjee, S., Sarkar, S., Altermann, W and Catuneanu O (eds) 2007. Atlas of Microbial Mat Features Preserved within the Siliciclastic Rock Record; Atlases in Geoscience, 311pp.

Schieber, J. (1998). Possible indicators of microbial mat deposits in shales and sandstones: examples from the Mid-Proterozoic Belt Supergroup, Montana, USA. *Sedimentary Geology,* 120:105–124.

Schieber, J. (1999). Microbial mats in terrigenousclastics: the challenge of identification in the rock record. *Palaios,* 14:3–12.

Semikhatov, M. A., Gebelein, C. D., Cloud, P., Awramik, S. M., and Benmore, W. C. (1979). Stromatolite morphogenesis: progress and problems: C*anadian Journal of Earth Sciences,* 16:992–1014.

Shi, X.Y., Zhang, C.H., Jiang, G.Q., Liu, J., Wang, Y., and Liu, D.B. (2008). Microbial mats in the Mesoproterozoic carbonates of the North China platform and their potential for hydrocarbon generation. *Geoscience* 22(5), 669-682.

Shields-Zhou, G. and Och, L. (2011). The case for a Neoproterozoic Oxygenation Event: Geochemical evidence and biological consequences. *GSA Today*, 21(3): 4-11. DOI: 10.1130/GSATG102A.1.

Shields, G., and Stille, P. (2001). Diagenetic constraints on the use of cerium anomalies as palaeoseawater proxies: an isotopic and REE study of Cambrian phosphorites. *Chemical Geology*, 175:29–48.

Sim, M.S., Liang, B., Petroff, A.P., Evans, A., Klepac-Ceraj, V., Flannery, D.T., Walter, M.R., and Bosak, T. (2012). Oxygen-dependent morphogenesis of modern clumped photosynthetic mats and implications for the Archean stromatolite record. *Geosciences,* 2:235–59.

Stille, P., Gauthier-Lafaye, F., Jensen, K.A., Gomez, P., Ewing, R., Louvat, D., 2000. REE migration in groundwaters close to the natural fission reactor or Bangombe' Gabon.; Sm–Nd isotope evidence. Earth Planet. Sci. Lett.

Sumner D. Y., Jungblut D., Hawes I., Andersen D. T., Mackey J., and Wall K. (2016). Growth of elaborate microbial pinnacles in Lake Vanda, Antarctic. *Geobiology* DOI: 10.1111/gbi.1218

Taylor, S.R., and McLennan, S.M. (1985). The Continental Crust; Its Composition and Evolution: London, Blackwell, p. 312.

Tostevin, R., Shields, G.A., Tarbuck, G.M., He, T., Clarckson, M.O., and Wood, R.A. (2016). Effective use of cerium as redox proxy in carbonate-dominated marine settings. *Chemical Geology,* 438:146–162.

Tribovillard, N., Algeo, T. J., Lyons, T., and Roboulleau, A. (2006). Trace metals as paleoredox and paleoproductivity proxies: An update. *Chemical Geology,* 232:12–32.

van Smeerdijk Hood, A., and Wallace, M.W. (2015). Extreme ocean anoxia during the Late Cryogenian recorded in reefal carbonates of Southern Australia, *Precambrian Research,* 261, 96–111.

Warren, L. V., Quaglio, F., Riccomini, C., Simões, M.G., Poiré, D.G., Strikis, N.M., Anelli, L.E., and Strikis, P.C., (2014). The puzzle assembled: Ediacaran guide fossil Cloudina reveals an old proto-Gondwana seaway. *Geology* 42(5), 391–394.

Webb, G.E., and Kamber, B.S. (2000). Rare earth elements in Holocene reefal microbialites: a new shallow seawater proxy. *Geochimica et CosmochimmicaActa* 64, 1557–1565. http://dx.doi.org/10.1016/S0016-7037(99)00400-7.

Wei, W., Frei, R., Gilleaudeaub, G.J., Wei, G.Y., and Linga, H.F. (2018). Oxygenation variations in the atmosphere and shallow seawaters of the Yangtze Platform during the Ediacaran Period: Clues from Cr-isotope and Ce-anomaly in carbonates. *Precambrian Research* 313 :78–90.

Wei, H. Wang, X., Shi, X., Jiang, G., and Tang, D. (2019). Iodine content of the carbonates from the Doushantuo Formation and shallow ocean redox change on the Ediacaran Yangtze Platform, South China. *Precambrian Research,* 322: 160–169.

Zhao, C., Shi, M., Feng, Q.,Ye, Y., Khan, M. Z., and Feng, F. (2020). New study of microbial mats from the Mesoproterozoic Jixian Group, North China: Evidence for photosynthesis and oxygen release, *Precambrian Research*, 344: 105-734, ISSN 0301-9268, https://doi.org/10.1016/j.precamres.2020.105734.